

# SYSTEM SENSITIVITY IN PRECLINICAL SMALL ANIMAL IMAGING

<sup>1</sup>Arion F. Chatziioannou, <sup>1</sup>Qinan Bao, <sup>2</sup>N. Karakatsanis

<sup>1</sup>Crump Institute for Molecular Imaging, University of California, Los Angeles, CA, USA

<sup>2</sup>Department of Electrical and Computer Engineering, NTUA, Athens, Greece

## ABSTRACT

Preclinical small animal imaging is an important tool at the disposition of biological researchers. While the range of studies performed by non-invasive preclinical imaging is greatly varied, high sensitivity is of key importance in any biological experiment with molecular imaging probes. The technologies that are used to achieve high system sensitivity mostly focus on the use of large solid angles and dense scintillator materials. In this work, we investigate and discuss different preclinical Positron Emission Tomography system designs and the effects of these designs on the overall sensitivity. We focus our investigations in hypothetical system geometries and scintillator materials and perform Monte Carlo simulations. The results indicate that preclinical PET systems based on detector materials that have minimal intrinsic background and higher effective atomic number, might offer performance advantages for situations where the weakest signal possible needs to be detected.

**Index Terms**— preclinical PET, small animal imaging, system sensitivity

## 1. INTRODUCTION

Tomographic systems dedicated to non-invasive imaging of preclinical animal models have become widely available in recent years [1, 2]. The initial thrust for the development of these systems coincided with the rise of the mouse as the favorite and predominant model of mammalian physiology [3]. In particular, the arrival of the genetically modified mouse has created a wealth of knowledge about the genetics of normal and diseased physiology. The ability to non-invasively and repeatedly image the same subject has strengthened the experimental protocols and enhanced our understanding of variations that naturally occur even between genetically identical subjects. Due to the vast differences in size between the laboratory mouse and an average human, dramatically improved spatial resolution was the obvious first and most important step in the design of dedicated rodent imaging PET systems, and has continued being the driving force behind new developments [4, 5].

Commercialization of these technologies has significantly increased the utility and flexibility of these original prototype high resolution imaging systems, providing whole body coverage, increased sensitivity and spatial resolution. Today, commercially available imaging systems boast ten to a hundredfold increased overall sensitivity from these early devices for imaging the laboratory mouse [6], as well as many other enhancements including multimodality imaging [7].

Most new imaging systems are based in novel scintillators with fast decay times that allow narrower coincidence timing windows, reduced pulse integration times and improved count rate capability. While these traits are important and useful for a successful implementation of a preclinical imaging system, high count rate capability is not in itself sufficient to bring the best performance possible in terms of low detection limits.

One of the key advantages of molecular imaging with PET is its capability to detect and measure non-invasively nano-molar to pico-molar concentrations of probes in-vivo. The small concentrations involved with most molecular markers indicate that a small number of radio-labeled molecules exist in-vivo and are available for detection. Higher system sensitivities for the detection of true events, in combination with lower system as well as biological background are the keys to this process.

The most common detector material used in small animal PET systems today is based on variants of <sup>176</sup>Lu silicates. These high light output, dense and fast scintillators have enabled the high spatial resolution necessary for imaging the laboratory mouse. As a drawback though, <sup>176</sup>Lu is intrinsically radioactive and produces constant coincidence system background that becomes increasingly significant at the limits of detection. Furthermore, the effective atomic number of LSO, the most common variant of this scintillator, is not as high as that of BGO, a more traditional scintillator. In this work, we will compare two hypothetical tomographs, one constructed out of BGO scintillator and another constructed out of LSO. A comparison between the important properties of the two types of scintillator for this work is in Table I.

TABLE I. Comparison of BGO and LSO scintillation crystals.

	<i>BGO</i>	<i>LSO</i>
Effective Atomic Number ( <i>Z</i> )	74.2	66
Density (g/cm <sup>3</sup> )	7.13	7.4
Light Yield (Photons/MeV)	8200	25000
Decay Constant ( $\mu$ s)	0.30	0.04

## 2. METHODS

### A. Monte Carlo platform

GATE, the GEANT4 Application for Tomographic Emission, is the Monte Carlo based simulation toolkit used in this study [8]. It encapsulates the well-proved GEANT4 libraries to achieve a modular and versatile simulation platform for PET and SPECT. With the capability to simulate the image

formation process in a wide range of tomographic systems, GATE is the tool that will assist us in the evaluation of the design of new imaging devices. The single and/or coincidence detections of gamma rays by the scintillation crystals were stored on an event-by-event basis and sorted into output files.

### B. The PET Systems

The geometries of the imaging systems modeled in this work were based on a hypothetical PET system dedicated to rodent studies. Our virtual PET scanner consisted of a ring of 16 scintillator detector arrays. Each array was made of crystals with sizes of  $1.5 \times 1.5 \times 10$  (15, 20) mm. The overall system had 80 crystal rings in total, and thereby an axial FOV of 12.7 cm (Fig. 1). The scanner operated in full 3D mode, producing 6400 sinograms (span 1) that included all ring differences (0-79) with 128 samples and 160 angles each.

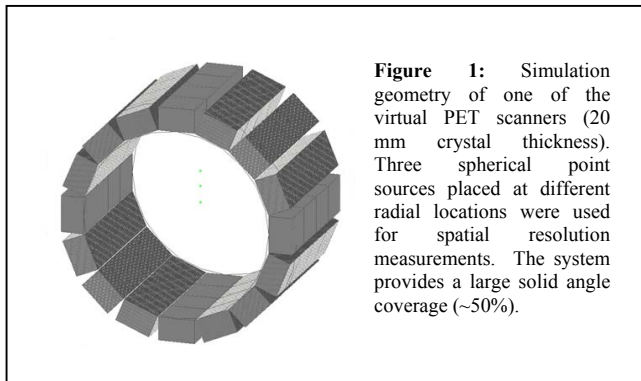


**Figure 1:** Simulation geometry of one of the virtual PET scanners (20 mm crystal thickness). Three spherical point sources placed at different radial locations were used for spatial resolution measurements. The system provides a large solid angle coverage (~50%).

### C. Detector Intrinsic Activity

For the LSO based tomograph, in addition to the source activity, we included the decay scheme of  $^{176}\text{Lu}$ , that produces  $\beta^-$  particles (420keV) in cascade with  $\gamma$  photons of energies of 307keV (94%), 202keV (78%) and 88keV (15%) [2]. We have measured that the total intrinsic activity of an LSO based system with similar geometry in the entire FOV volume to be approximately  $4\mu\text{Ci}$ . When a source with activity on the order of tens of nCi is imaged, then the standard deviation of background originating from the scintillator crystals can significantly raise the detection limit. Consequently the ability to detect point sources within a uniform background activity region is also adversely affected [9, 10].

### D. System Sensitivity

A  $10\mu\text{Ci}$   $^{18}\text{F}$  spherical point source of diameter 0.3 mm was placed inside of a water sphere of 4 mm diameter at the center of the PET system and simulated for a 3 second acquisition and for three crystal thicknesses: 10, 15 and 20 mm. A 250-750 keV energy window and a 12 ns timing window were used in the simulation. The absolute system sensitivities were calculated based on the number of true coincidences obtained in each simulation and the 96.73% positron yield of the  $^{18}\text{F}$  source.

### E. Radial and Tangential Resolution

To evaluate the effect of increased crystal depth on the spatial resolution of the hypothetical PET tomographs, we measured spatial resolution with the simulation of point sources in different locations in the field of view. For each crystal thickness (10, 15 and 20 mm),  $^{18}\text{F}$  point sources located at three different radial offsets 0 mm, 15 mm and 28 mm (Fig. 1) were simulated at 250-750keV energy window and 12 ns timing window. Each 0.3mm diameter spherical point source had an activity of  $10\mu\text{Ci}$  and was simulated for 10 second acquisitions. The  $^{18}\text{F}$  ion source was used in the simulation, to model positron range and photon non-collinearity.

A 2D filter backprojection (FBP) with a ramp filter cutoff at the Nyquist spatial sampling frequency was used to reconstruct the images. For simplicity, only one central sinogram was reconstructed, ignoring image reconstruction artifacts stemming from the large axial acceptance angles assumed in our sensitivity simulations. Radial and tangential profiles for each point source were drawn and each peak was fitted to a Gaussian function to determine the resolution in terms of full width at half maximum (FWHM).

### F. Scatter Fraction

The scatter fraction was evaluated by a small animal phantom, containing a line source insert. The cylindrical mouse-like phantom composed of water equivalent material had a diameter of 25 mm, a length of 70 mm and was placed at the center of the scanner. A line source that contained  $50\mu\text{Ci}$   $^{18}\text{F}$  was inserted parallel to the central axis at a radial distance of 10 mm. The line source insert had a diameter of 2.1 mm and a length of 70 mm. The simulation was performed at a 250-750 keV energy window with the assumption of 25% energy resolution at the reference 511 keV peak. For comparison, the same phantom inside an equivalent LSO based system was simulated with the assumption of 18% energy resolution for 511 keV peak.

The *phantom scatter fraction* was calculated by the ratio of scattered coincidences over true coincidences inside the object. The *crystal scatter fraction* was estimated by the ratio of crystal scattered coincidences over the total (crystal scattered coincidences + unscattered coincidences).

## 3. RESULTS

### A. System Sensitivity

The resulting sensitivities of the PET systems at the 250-750 keV energy window with different crystal thicknesses are summarized in Table II.

As the crystal thickness increased, more annihilated 511 keV photons were stopped in the detectors, more coincidences were detected and therefore higher sensitivity was achieved. The system absolute peak sensitivity was higher than 25% with 20 mm thick BGO crystals. This very high sensitivity was partially achieved because the BGO scintillator has higher effective atomic number and consequently a higher stopping power than LSO.

TABLE II. System sensitivities of the PET systems with different crystal thicknesses.

Crystal Thickness	10 mm	15 mm	20 mm
LSO sensitivity (%)	9.0	15.8	21.5
BGO sensitivity (%)	11.6	19.3	25.5

### B. Spatial Resolution

Due to our interest in mouse imaging, the chosen radial offsets were small. As a result, the FWHM measured tangential and radial components of the spatial resolution were not significantly different from each other. For simplicity and compactness we report here only the effective FWHM spatial resolution, with radial and tangential components added in quadrature. The resulting FWHM spatial resolutions for the LSO and BGO imaging systems, at measured radial offsets of 0, 15 and 28 mm from the center of the FOV are summarized in Table III.

The FWHM resolution became progressively worse as the crystal thickness increased and as the source moved towards off-center positions. It is important to note that the FWHM measured for the LSO and BGO tomographs were comparable, but the spatial resolution for the BGO system was systematically better than that of LSO as the crystals became longer. While we are not reporting here the full width at tenth maximum (FWTM) between the LSO and BGO systems, we need to mention that the same trend is observed, but much more significant. In LSO systems, due to the larger amount of inter-crystal scatters, the point spread function (PSF) usually has long tails, which largely increases the FWTM. The PSF for BGO systems with less crystal scatter has shorter tails and the resulted smaller FWTM is important for low contrast detection.

Table III. Transverse image plane spatial resolution (FWHM) for the PET systems with different crystal thicknesses.

Offset (mm)	0			15			30		
	10	15	20	10	15	20	10	15	20
Crystal length	10	15	20	10	15	20	10	15	20
LSO (mm)	2.0	2.2	2.2	2.5	2.8	3.3	2.6	3.1	3.7
BGO (mm)	2.0	2.0	2.1	2.5	2.6	2.9	2.7	2.8	3.4

### C. Scatter Fraction

*Phantom scatter:* The scatter fraction inside of the mouse-size phantom was estimated to be 4.5% with an energy window of 250-750 keV. By increasing the lower level discriminator, the scatter fraction can be reduced at the expense of reduced system sensitivity. The scatter profile of a line source inside a mouse size phantom is shown in Fig. 2. With the equivalent

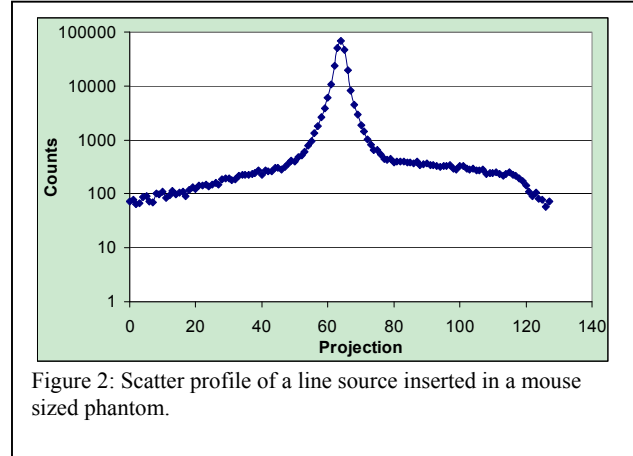


Figure 2: Scatter profile of a line source inserted in a mouse sized phantom.

LSO scanner, the scatter due to the phantom was 4.6%, which was similar to that of the BGO scanner at the energy window evaluated.

*Inter-crystal scatter:* In the BGO system, the average number of Compton interactions before the photon was fully absorbed or escaped was 0.68. With the equivalent LSO system, 0.85 Compton interactions were necessary. The inter-crystal scatter fraction with respect to total coincidences was approximately 10% higher with the LSO system than the BGO. Higher crystal scatter results inaccurate positioning and therefore, degrades the spatial resolution. The differences are most pronounced in the changes in the FWTM spatial resolution.

## 4. DISCUSSION

The advantages of LSO crystals are their high light output per absorbed unit energy and their fast light decay. The light yield of LSO is 3 times of BGO and therefore detectors based on LSO have better energy resolution. The increased light output makes these small crystals easier to identify in a segmented detector, increasing the potential for higher spatial resolution. Additionally, the faster light decay of LSO results lower system deadtimes at the same activity levels. Also, narrower timing windows can be used for LSO PET scanners and thus the number of random coincidences can be reduced and better count rate performance is achieved. These are important advantages, and the significance of most of them is large for clinical PET studies. In contrast, provided that the scintillators produce adequate signal for proper identification of the correct crystal of interaction, the significance of these advantages is diminished for small mouse sized objects. Conversely, the biggest advantages of BGO scintillator crystals are their high effective atomic number ( $Z$ ) and low intrinsic background. High  $Z$  increases the probability of photoelectric effect at the first interaction site, which means full absorption of the photon energy in one crystal. In small animal PET scanner, which requires the highest possible spatial resolution, the crystal size needs to be kept small. However, small crystal size increases the inter-crystal scatter and results incorrect positioning of the event. With the high effective atomic number of the BGO

scintillator, full absorption in one interaction reduces this effect. Therefore crystals can be made longer to increase system sensitivity. Even with the same crystal thickness though, the BGO scanner had higher system sensitivity than the LSO. Further improvement in sensitivity could be achieved by using thicker crystals without significantly sacrificing the spatial resolution for mouse studies. Transverse spatial resolutions were comparable to the LSO based system and in fact were better for the BGO based system. At the evaluated energy window of 250-750 keV, the phantom scatter fraction was similar, while the crystal scatter fraction was about 10% lower. Additionally, the lack of intrinsic coincidence background when BGO crystals are used should directly improve the minimum level of detectable activity. In other related work, the lower energy discriminator window had to be raised significantly, to reduce the rate of intrinsic coincidences [9]. The result of this energy windowing has a direct and significant negative impact on the absolute system sensitivity, especially when imaging is performed close to the limits of detection.

## 5. CONCLUSION

Small animal PET scanners based on LSO and BGO scintillator materials were simulated. For low level activity detection, the BGO based system had higher overall sensitivity, reduced crystal scatter and improved spatial resolution than the equivalent LSO based scanner. While it is known that longer crystals degrade event positioning accuracy and spatial resolution, BGO crystals reduced inter-crystal scatter and made thicker detectors acceptable. This in turn allows the design of systems with even higher sensitivity and with resolution acceptable for mouse studies. While the axial crystal penetration was not evaluated in this work, in the future we plan to fully reconstruct the point source simulations. This way, we will get more accurate estimations of the FWHM and FWTM in radial, tangential and axial directions and get the volumetric resolutions of different positions in the FOV. Compared with the LSO scintillator, BGO has a much longer decay constant. This can be a problem at high count rate as the system will suffer significant counts loss due to deadtime. However, small animal PET scans are usually performed at relatively low injected activities to avoid unnecessary radiation dose [11]. The injected activity for tumor models is usually on the order of 100  $\mu$ Ci, which is far from the activity level for peak NECR. With the increased system sensitivity of the BGO system, the injected activity can be further reduced. The wider timing window needed due to the slow light decay, results in higher random coincidences but this should not be an important consideration for small amounts of injected activity.

The  $^{176}\text{Lu}$  in LSO crystals has an intrinsic radioactivity, which will be a problem for imaging low uptakes in mouse targets. BGO scintillators do not have any intrinsic radioactivity and with the higher system sensitivity, it might be more suitable for imaging small amount of activities inside of animals.

## 6. ACKNOWLEDGEMENTS

The authors would like to acknowledge discussions with Harvey Herschman, Richard Taschereau, Sam Gambhir, David Stout, Caius Radu, and Jenny Shu in the preparation of this manuscript. Funding was provided in part by a National Institutes of Health cooperative agreement UCLA SAIRP NIH-NCI 2U24 CA092865.

## REFERENCES

- [1] A. F. Chatziioannou, "Molecular imaging of small animals with dedicated PET tomographs," *European Journal of Nuclear Medicine*, vol. 29, pp. 98-114, Jan 2002.
- [2] H. R. Herschman, "Molecular imaging: Looking at problems, seeing solutions," *Science*, vol. 302, pp. 605-608, Oct 24 2003.
- [3] D. Malakoff, "The rise of the mouse, biomedicine's model mammal," in *Science*, vol. 288, 2000, pp. 248-253.
- [4] A. Chatziioannou, Y. C. Tai, N. Doshi, and S. R. Cherry, "Detector development for microPET II: a 1 m $\mu$ l resolution PET scanner for small animal imaging," *Physics in Medicine and Biology*, vol. 46, pp. 2899-2910, Nov 2001.
- [5] J. R. Stickel, J. Y. Qi, and S. R. Cherry, "Fabrication and characterization of a 0.5-mm lutetium oxyorthosilicate detector array for high-resolution PET applications," *Journal of Nuclear Medicine*, vol. 48, pp. 115-121, Jan 2007.
- [6] Y. C. Tai, A. Ruangma, D. Rowland, S. Siegel, D. F. Newport, P. L. Chow, and R. Laforest, "Performance evaluation of the microPET focus: A third-generation microPET scanner dedicated to animal imaging," *Journal of Nuclear Medicine*, vol. 46, pp. 455-463, Mar 2005.
- [7] S. R. Cherry, "Multimodality in vivo imaging systems: Twice the power or double the trouble?," *Annual Review of Biomedical Engineering*, vol. 8, pp. 35-62, 2006.
- [8] S. Jan, G. Santin, D. Strul, S. Staelens, K. Assie, D. Autret, S. Avner, R. Barbier, M. Bardies, P. M. Bloomfield, D. Brasse, V. Breton, P. Bruyndonckx, I. Buvat, A. F. Chatziioannou, Y. Choi, Y. H. Chung, C. Comtat, D. Donnarieix, L. Ferrer, S. J. Glick, C. J. Groiselle, D. Guez, P. F. Honore, S. Kerhoas-Cavata, A. S. Kirov, V. Kohli, M. Koole, M. Krieguer, D. J. van der Laan, F. Lamare, G. Langeron, C. Lartizien, D. Lazaro, M. C. Maas, L. Maigne, F. Mayet, F. Melot, C. Merheb, E. Pennacchio, J. Perez, U. Pietrzyk, F. R. Rannou, M. Rey, D. R. Schaart, C. R. Schmittlein, L. Simon, T. Y. Song, J. M. Vieira, D. Visvikis, R. Van de Walle, E. Wieers, and C. Morel, "GATE: a simulation toolkit for PET and SPECT," *Phys Med Biol*, vol. 49, pp. 4543-61, Oct 7 2004.
- [9] A. L. Goertzen, J. Y. Suk, and C. J. Thompson, "Imaging of Weak-Source Distributions in LSO-Based Small-Animal PET Scanners," *J Nucl Med*, vol. 48, pp. 1692-1698, October 1, 2007.
- [10] C. C. Watson, M. E. Casey, L. Eriksson, T. Mulnix, D. Adams, and B. Bendriem, "NEMA NU 2 performance tests for scanners with intrinsic radioactivity," *Journal of Nuclear Medicine*, vol. 45, pp. 822-826, May 2004.
- [11] R. Taschereau and A. F. Chatziioannou, "Monte carlo simulations of absorbed dose in a mouse phantom from 18-fluorine compounds," *Med Phys*, vol. 34, pp. 1026-1036, March 2007.